Revista Brasileira de Geografia Física v.14, n.05 (2021) 3078-3095

Revista Brasileira de Geografia Física

ISSN:1984-2295

Homepage: https://periodicos.ufpe.br/revistas/rbgfe

Satellite-Derived Bathymetry models from Sentinel-2A and 2B in the coastal clear waters of Arraial do Cabo, Rio de Janeiro, Brazil

Ruan Vargas[1], Julio Cesar de Faria Alvim Wasserman[2], Alberto Luis da Silva[3], Thiago Leal Tavares[4], Camila Américo dos Santos[5], Fábio Ferreira Dias[6,7]

1Doctoral Student, Marine Biology and Coastal Environments Postgraduate Program - PBMAC, Biology Institute, UFF - Federal Fluminense University, Outeiro São João Batista Street, Niterói, Rio de Janeiro, Brazil, CEP: 24020-971, ruanvargas@id.uff.br (corresponding author). [2]Professor in Graduate Program in Geoscience (Geochemistry), UFF – Federal Fluminense University, Niterói, Rio de Janeiro, Brazil, julio.wasserman@gmail.com. [3]IBGE - Brazilian Institute of Geography and Statistics, Rio de Janeiro, Brazil, albertosilva@vm.uff.br. [4]Master Student, Biosystems Engineering Postgraduate Program - PGEB, UFF – Federal Fluminense University, Passo da Pátria Street, 156, São Domingos, Niterói, Rio de Janeiro, Brazil, CEP: 24210-240, thiagoleal@id.uff.br. [5]Master in Biosystems Engineering Postgraduate Program - PGEB, UFF – Federal Fluminense University, camilaamerico@id.uff.br. [6]Professor in Marine Biology and Coastal Environments Postgraduate Program - PBMAC, Biology Institute, UFF - Federal Fluminense University, fabioferreiradias@id.uff.br. [7]Professor in Biosystems Engineering Postgraduate Program - PGEB, UFF – Federal Fluminense University.

Artigo recebido em 12/05/2021 e aceito em 27/07/2021

A B S T R A C T

Remote sensing offers a practical alternative for extracting depth information, obtaining a fast, repetitive and low-cost mapping over large areas to optimize and minimize field work. This study aims to generate Satellite-Derived Bathymetric (SDB) models from Sentinel-2A and 2B images on Praia dos Anjos, Brazil. The log-transform band ratio model was applied in this study. Two images from Sentinel-2 were used, from April 6, 2019 and June 20, 2019. For calibration and validation of SDB, depths were measured in the field with an echosounder on April 4, 2019. Different intervals of depths were tested, and the red wavelength to estimate depths up to 4 m. The statistical correlation between the image and control points on April 6, was r^2 = 0.927 for 1-13 m depth interval and between SDB and check points was r^2 = 0.893 with a Root Mean Square Error (RMSE) = 1.095. On June 20, the correlation between image and control points was r^2 = 0.938 for 1-13 m depth interval, and between SDB and check points was r^2 = 0.919 with a RMSE = 0.98. This study showed that remote sensing can be applied to estimate depths on Praia dos Anjos. Bathymetric information is essential for environmental monitoring and coastal engineering works. Further tests in the area are recommended to improve the models and an assessment of the calibrated equations for future applications with new measured check points.

Key words: remote sensing, coastal environments, echo sounding, empirical algorithm, Angels Beach

Modelos batimétricos derivados dos satélites Sentinel-2A e 2B nas águas claras costeiras de Arraial do Cabo, Rio de Janeiro, Brasil

R E S U M O

O sensoriamento remoto oferece uma alternativa prática para extrair informações de profundidade, obtendo um mapeamento rápido, repetitivo e de baixo custo para otimizar o trabalho de campo. Este estudo tem como objetivo gerar modelos batimétricos derivados de satélites (SDB) a partir de imagens Sentinel-2A e 2B na Praia dos Anjos, Brasil. O modelo de razão de banda de transformação logarítmica foi aplicado neste estudo. Duas imagens do Sentinel-2 foram usadas, de 6 de abril de 2019 e 20 de junho de 2019. Para calibração e validação do SDB, profundidades foram medidas em campo com uma ecossonda em 4 de abril de 2019. Diferentes intervalos de profundidades foram testados e o comprimento de onda vermelho para estimar profundidades de até 4 m. A correlação estatística entre a imagem e os pontos de controle em 6 de abril foi r^2 = 0,927 para o intervalo de profundidade de 1-13 m e entre o SDB e os pontos de verificação foi r^2 = 0,893 com uma Raiz do Erro Quadrático Médio (RMSE) = 1,095. Em 20 de junho, a correlação entre a imagem e os pontos de controle foi r^2 = 0,938 para o intervalo de profundidade de 1-13 m, e entre o SDB e os pontos de verificação foi r^2 = 0,919 com RMSE = 0,98. Este estudo mostrou que o sensoriamento remoto pode ser aplicado para estimar profundidades na Praia dos Anjos. A informação batimétrica é essencial para o monitoramento ambiental e obras de engenharia costeira. Outros testes na área são recomendados para aprimorar os modelos e uma avaliação das equações calibradas em futuras aplicações com novos pontos de verificação medidos.

Palavras-chave: sensoriamento remoto, ambientes costeiros, ecossondagem, algoritmo empírico, Praia dos Anjos.

Introduction

The mapping of underwater relief and depth measurements in coastal and marine environments appeared with the historical need to recognize submerged features, to promote safe navigation and to create nautical charts (Smith and Sandwell, 2004). Currently, this knowledge is applied for several purposes such as monitoring coastal erosion (e.g. Henrico and Bezuidenhout, 2020) mapping and monitoring coastal ecosystems (e.g. Conti et al., 2020), coastal engineering projects (e.g. Bitan and Zviely, 2020), dredging (e.g Venancio et al., 2020), environmental monitoring programs and management of port facilities (e.g. Mateo-Pérez et al., 2020).

There are several techniques and methods to measure depths of a water body. These can be classified into acoustic (echo sounding in various frequencies) and non-acoustic (LIDAR; International Hydrographic Organization – IHO, 2005). The most reliable and attaining all depths is echo sounding (single beam or multibeam systems) which is broadly used worldwide. However, hydrographic surveys carried out by echo sounding and LIDAR are regarded as expensive and time-consuming methodologies (Leder et al., 2019).

With the improvement and development of new technologies, such as Global Navigation Satellite System (GNSS), Geographic Information System (GIS) softwares and mainly the satellites and its sensors, hydrographic and bathymetric surveys were further improved (Simões, 2007). Remote sensing offers a promising and practical alternative method for obtaining depth information, producing fast, repetitive and low-cost mapping over a large area, optimizing and minimizing field work (Jagalingam et al., 2015; Casal et al., 2019).

Methodologies for Satellite-Derived Bathymetry (SDB) have been developed since the 1970s (Lyzenga, 1978) and, consequently, improved over time (Caballero and Stumpf, 2019, 2020). With the advent of satellites like Landsat series and recently, the European Sentinel-2 mission, in addition to other satellites as the Worldview family, IKONOS and QuickBird, the images have been extensively evaluated and tested worldwide. Applying different wavelengths of electromagnetic radiation, different coastal environments could be successfully surveyed (e.g. Jagalingam et al., 2015; Parente and Pepe, 2018; Caballero and Stumpf, 2019; Basith and Prastyani, 2020; Conti et al., 2020; Simpson et al., 2021; Wei and Theuerkauf, 2021; Westley, 2021). Indeed, according to Evagorou et al. (2019) new studies applying SDB show the potential of remote sensing for bathymetric mapping purposes using different approaches, being able to estimate depths up to 30 meters.

The quality of the radiometric bathymetry depends on a series of factors related to imaging by the remote sensor such as solar elevation and platform height, as well as environmental factors related to the water itself as waves, roughness, clarity, in-water constituents, light scattering, light attenuation and depth. Nevertheless, the main factor that affects the quality of the bathymetric model generated by satellites is turbidity (Gao, 2009). Therefore, SDB accuracy is usually expressed by the coefficient of determination r2 of the regression model and error analysis (Gao, 2009).

Remote sensing has become a useful tool for coastal managers worldwide. Mumby and Edwards (2000) applied a questionnaire considering several remote sensing techniques used in the coastal zone. Sixty managers from many countries pointed out that the most common utilities (primary applications) was to provide background information for planning (more than 60%), equaling with detecting change in habitats over time and followed by monitoring strategies of planning.

Although, SDB is still poorly explored in Brazil, and it is certainly a promising technique, mainly in developing countries, where resources are scarce. This study aims to generate and evaluate bathymetric models from Sentinel-2 satellite images and their application in a coastal embayment in the municipality of Arraial do Cabo, Brazil. It is expected that the survey constitutes a contribution to monitoring changes in wave-induced shallow geomorphological features.

Material and methods

Study area

Praia dos Anjos (Angels Beach) is located in the municipality of Arraial do Cabo, east of the state of Rio de Janeiro (RJ), southeast Brazil (Figure 1). Currently, this beach has a length of approximately 1,200 m and a rock breakwater that shelters the Forno Port and a boat marina for artisanal fishermen and tourism. The breakwater closes the entrance of the cove in about 35% of its cross section and probably cause a severe geomorphological impact on the beach. It is recognized that the morphodynamic processes of the beach were altered by the breakwater and, associated with the anthropic occupations, resulted in erosion in the southern region of the beach (Savi, 2007; Colaço et al., 2021).

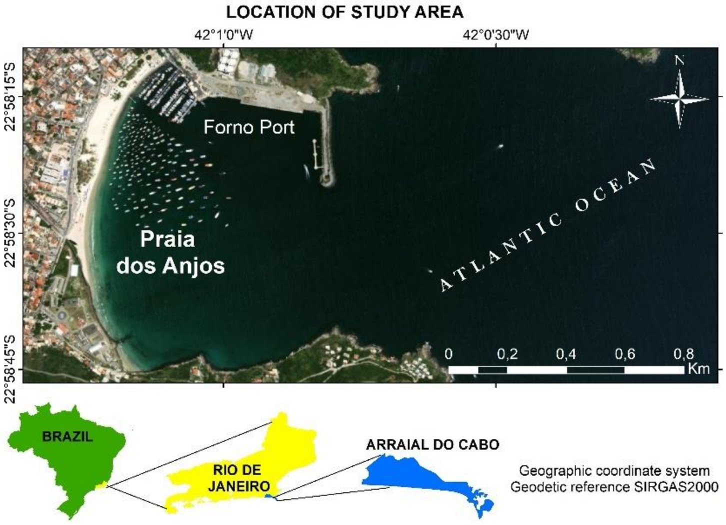

Figure 1. Location of study area. Praia dos Anjos.

Geographically, Arraial do Cabo is a turning point of the Brazilian coast, abruptly changing the alignment from northeast-southwest to east-west (Motta et al., 2018; Colaço et al., 2021). The region has a warm semiarid climate, considered a “phytogeographic enclave” within RJ, which has a humid tropical climate (Barbiére, 1975; Coe and Carvalho, 2013).

The region is included in “Bacia de Campos” geological microcompartment (Muehe, 1998). It corresponds to an important pre-salt oil and gas reservoir located on the continental shelf of Brazil, bounded on the north by the “Bacia do Espírito Santo” (state of Espírito Santo) and on the south by “Bacia de Santos” (state of São Paulo), which the coverage area is approximately 100,000 km2 (Figueiredo Jr et al., 2015; Habermann et al., 2018). This compartment is located between the 10 and 150 m isobaths and its formation is related to the rupture (rifting) process of the Gondwana paleocontinent, the separation from the African and South American continents, where it would have started in Cretaceous approximately 130 million years ago (Riccomini et al., 2012; Figueiredo Jr et al., 2015).

The meteorological picture is dominated by northeast winds and waves, with northeast quadrant undulations associated with the South Atlantic Subtropical Anticyclone (SASA). During cold front systems and extratropical cyclones, the occurrence of storm surges and destructive waves from southwest-south quadrant is recorded (Dias et al., 2014; Quadros et al., 2016). According to Silva (2009) the tide is asymmetrical and semi-diurnal, with an amplitude of approximately 1.0 meter in spring tide.

The main oceanographic characteristic of Arraial do Cabo is the upwelling, a local phenomenon attributed to the configurations of the coast and the northeast winds. This phenomenon is related to a divergence of the coast and the Brazil Current (a superficial hot ocean current) that comes from the Equator, favoring the upwelling between September (spring) and March (summer). During fall and winter, the inverse phenomenon occurs, the downwelling, as a response to the southwest-south winds. The frequent upwelling implies a reduction of precipitation, increase of evaporation and salinity of nearby coastal lagoons and beaches, producing a drier climate (Barbosa et al., 2003, Melo et al., 2009; Coe and Carvalho, 2013; Areias et al., 2020).

Estimating depth by satellite remote sensing data

The fundamental principle for depth estimation by remote sensing techniques is that different wavelengths of the electromagnetic spectrum penetrate in the water with different intensities (Green et al., 2000; Gao, 2009). Thus, the most obvious characteristic that an orbital image can indirectly provide is the depth and shape of the submerged relief through its colors or tonalities. Shallower areas will reflect light more intensely, appearing brighter in the image, while deeper areas will reflect less radiation and, consequently, appear darker (Green et al., 2000).

The range of the electromagnetic spectrum that most penetrates in water is the blue light (0.4 to 0.5 µm) which this wavelength can penetrate in a water body for at least 25m (Caballero and Stumpf, 2019). Accordingly, Gao (2009) states that optical bathymetry takes advantage of the wavelengths of blue and green, which have a greater ability to penetrate in water. On the other hand, the red light is attenuated more quickly than smaller wavelengths (Mumby and Edwards, 2000). Thus, considering the water without the presence of optically active components (phytoplankton, suspended sediments and dissolved organic substances), as the wavelength increases, its reflectance decreases (Novo, 2010).

The methodology applied in this study was based on past studies published in the scientific literature (Table 1). Among them, the log-transform band ratio model developed by Stumpf et al. (2003), widely applied, was used. According to Zwolak et al. (2020) this is a modern and main methodological reference for bathymetric mapping used with different satellites and sensors.

Table 1 - Examples of Satellite-Derived Bathymetry studies and different methodologies, environments and data.

Authors	**Country - Environment**	**Images**	**Atmospheric correction**	***In situ* data**	**Methods**
Casal et al. (2019)	Ireland - Bay	Sentinel-2 Level-1	Yes	Multibeam echo sounder and lidar	Lyzenga (1978) and Stumpf et al. (2003)
Evagorou et al. (2019)	Cyprus – Sandy beach	Sentinel-2 Level-2	Yes	Multibeam echo sounder and lidar	Stumpf et al. (2003)
Jagalingam et al. (2018)	India - Low wave energy environment	Landsat 8	No	Nautical charts	Stumpf et al. (2003)
Guerreiro and Moura (2015)	Portugal – Tidal inlet lagoon	Landsat 8 Level-1	Yes	Echo sounder	Stumpf et al. (2003)
Stumpf et al. (2003)	USA – Coral reef, atol	Ikonos	Yes	Lidar	Lyzenga (1978);

					Stumpf et al. (2003)
Leder et al. (2019)	Croatia - Murter Island - Adriatic Sea	Landsat 8 and Sentinel- 2	No	Nautical charts	Stumpf et al. (2003)
Caballero and Stumpf (2019)	USA – Coral islands, limestone archipelago, barrier island beach	Sentinel-2	Yes	Lidar and nautical charts	Stumpf et al. (2003)
Abualhin and Niemeyer (2018)	Gaza Strip - Coastal zone	QuickBird	Yes	Nautical charts	Jupp (1988); Stumpf et al. (2003)
Tang and Mahmud (2018)	Malasya - Strait of Johor	Landsat 8	Yes	Nautical charts and echo sounding	Stumpf et al. (2003); Dierssen et al. (2003)
Kimeli et al. (2018)	Kenya – Mombasa Port Channel	Landsat 8	Yes	Nautical charts	Stumpf et al. (2003); Dierssen et al. (2003)
Chénier et al. (2018)	Canada – Artic Sea, Bays	Worldview -2 and 3	No	Multibeam echo sounder, lidar and leadline	Lyzenga (1985) ; Stumpf et al. (2003)
Conti et al. (2020)	Brazil – Estuarine Bay	Worldview -2	Yes	Singlebeam echosonder	Stumpf et al. (2003)

The applied method is empirical and based on statistical relationships between radiometric values of the pixels and known depths (Stumpf et al., 2003; Gao, 2009). Thus, estimating bathymetry using empirical models requires an adequate selection of spectral wavelengths, model construction and validation (Gao, 2009). Figure 2 represents the global methodology applied in this study.

Satellite data: Sentinel-2A/B images

In this study, images from the European Space Agency (ESA) Sentinel-2 mission were used. The Sentinel-2 mission comprises twin satellites describing polar orbits and synchronized with the sun (Sentinel-2A and 2B), phased at 180 ° from each other, with an average altitude of 786 km and positions measured by dual-frequency GNSS (ESA, 2015).

The Sentinel-2A satellite was launched on June 23, 2015 and 2B on March 7, 2017 (ESA, 2015; Caballero and Stumpf, 2019). The two satellites operate simultaneously and provide a temporal resolution of 5 days in Equator (or 10 days with one satellite) and 2-3 days in medium latitudes. The limits of imaged coverage are between 56 ° South and 84 ° North (ESA, 2015).

Sentinel-2 satellites operate passively collecting the reflected energy from Earth's surface, equipped with the Multispectral Instrument (MSI) in which it provides 13 spectral bands, 4 of them are 10m spatial resolution; 6 bands are 20m and 3 bands are 60m and 12 bits of radiometric resolution images (ESA, 2015).

Sentinel-2 satellites operate passively collecting the reflected energy from Earth's surface, equipped with the Multispectral Instrument (MSI) in which it provides 13 spectral bands, 4 of them are 10m spatial resolution; 6 bands are 20m and 3 bands are 60m (Table 2) and 12 bits of radiometric resolution images (ESA, 2015).

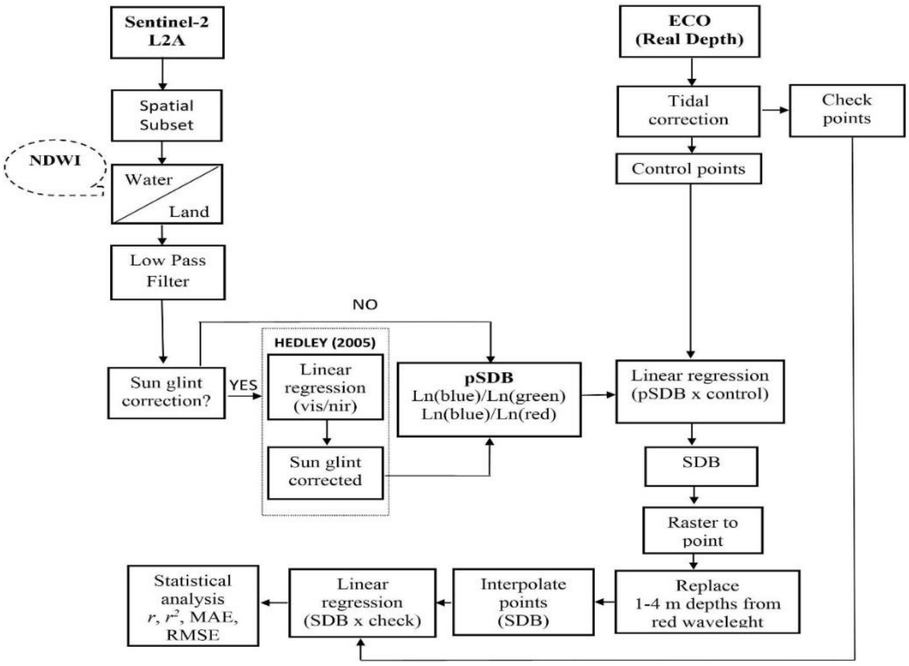

Figure 2. Methodological flow used to generate satellite-derived bathymetric models on Praia dos Anjos. Adapted from Guerreiro and Moura (2015).

Table 2 - Sentinel-2 MSI characteristics. Spectral and spatial resolutions. Adapted from Caballero and Stumpf (2019).

Band Number	Central Wavelenght (nm)	Bandwidth (nm)	Spacial Resolution (m)
1	443	20	60
2	490	65	10
3	560	35	10
4	665	30	10

5	705	15	20
6	740	15	20
7	783	20	20
8	842	115	10
8b	865	20	20
9	945	20	60
10	1375	30	60
11	1610	90	20
12	2190	180	20

The images were acquired from the ESA website where they are free available (https://scihub.copernicus.eu/dhus/#/home). As described by Evagorou et al. (2019), processed images in Level-2A, Bottom-of-Atmosphere (BOA) reflectance and orthorectified in UTM coordinate system (WGS84) were used. Thus, the images are provided with radiometric, geometric and atmospheric corrections.

Two images, one from each satellite, were selected for two different dates: one in April 6, 2019 (Sentinel-2A) and another in June 20, 2019 (Sentinel-2B). The selection of images was based on the absence clouds cover in the scene, mainly over the study area; absence or low presence of sunglint effects; and proximity to the date of the field research. However, only the blue (490 nm), green (560 nm), red (665 nm) and near infrared (842 nm) bands were used for the generation of bathymetric models throughout the processing.

In situ data: echo sounding

The field data used for calibration and validation of the bathymetric models were measured on April 4th 2019 according to the methodology applied by Carvalho et al. (2018) and Vargas et al. (2020). This methodology allows to normalize the depth points to the mean sea level (MSL) or mean lowest low water (MLLW – local reduction level), eliminating the effect of the tide. For depth measurements, it was used a single-beam echo sounder in a vessel and two GNSS receptors (geodetic) for geographic coordinates records from Differential Global Positioning System (DGPS) technique. In addition to the geographic coordinates, the receptors provided the ellipsoidal altitudes (h) related to the geodetic reference WGS84, necessary for elimination of tide effects.

One of the GNSS receptors was associated with the echo sounder (fixed in the hull of the boat), operating in kinematic mode (rover), and the vertical distance measured between the sounder and the receptor was 2.05 m. The other receptor was fixed at the SAT GPS 91783 station of the Brazilian Institute of Geography and Statistics (IBGE) (http://www.bdg.ibge.gov.br/bdg/pdf/relatorio.asp?L1=91783) (22° 58` 42.48583``S and 42° 01` 12.94081``O).

The data recorded by both GNSS receptors were unloaded for post-processing in GTR Processor software. This processing resulted in a table with time, latitude, longitude and ellipsoidal altitude information in WGS84 geodetic reference system for each point recorded.

After post-processing the GNSS receptors, the exported table of the echo sounder was associated with the information from the kinematic GNSS receptor table through the hour of tracking (hour, minute, second). At end, it resulted in a single table containing information of latitude, longitude, ellipsoidal altitude, and depth. For processing purposes, the GRS80 ellipsoid was considered the same as WGS84, both geocentric systems. The values of each uncorrected depth point could be reported to the MLLW (Carvalho et al., 2018; Vargas et al., 2020):

$$D_{(t)} = P_{(t)} - h_{(t)} + N + L \quad (1)$$

where $D_{(t)}$ is the corrected MLLW depth in meters at instance t; $P_{(t)}$ is uncorrected depth at instance t; $h_{(t)}$ is the ellipsoidal altitude at instance t; N is the geoid undulation = -5.8787 m for the area; and L is a constant = -0.5197 m, the local difference between the MLLW and MSL.

The measured depths referenced to the MLLW were considered as "real" and were randomly separated between control and check points distributed throughout the area (Figure 4). The control points were used to calibrate the satellite images described below, while the check points were later used for validation and statistical analysis.

Log-transform band ratio algorithm

For the application of the log-transform band ratio algorithm developed by Stumpf et al., (2003), first it is necessary to identify water/land separation, perform spatial image filtering and sun glint correction in the images (Leder et al., 2019). All of the following processing was done using ArcGIS 10.0 and Excel softwares.

Initially, the satellite images were resized to cover just the area of interest (Praia dos Anjos, Figure 1). Then, the NDWI was calculated to separate water and land features (McFeeters, 1996). This spectral index is contained in a range from -1 to +1 where radiometric values > 0 represent water and ≤ 0 land. In this way, the non-water features in the image could be excluded from processing, excluding boats in the area (Figure 5).

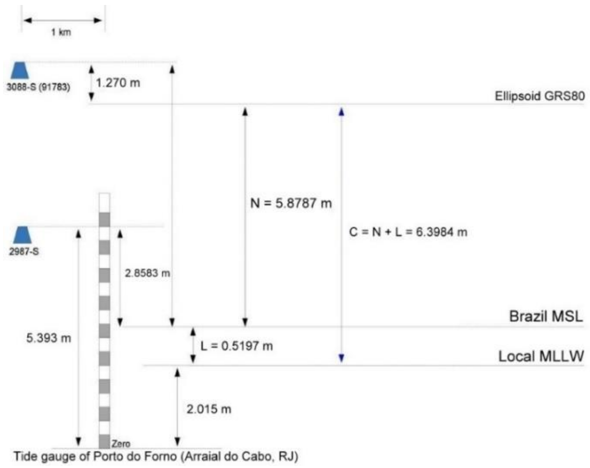

Figure 3. Topographic relationships representing the N and L constants values for tidal correction to MSL or MLLW in bathymetric surveys. Adapted from Vargas et al. (2020).

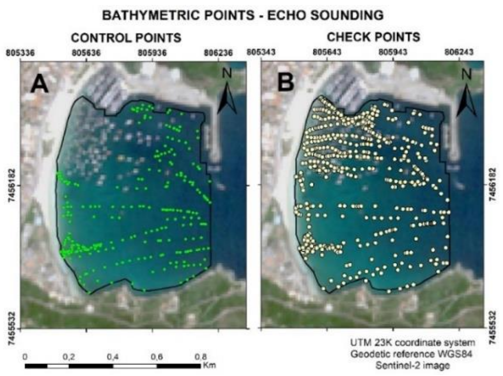

Figure 4. Depth points measured in field on April 4, 2019, using a single beam echo sounder. (A) Control points used to calibrate the models. (B) Check points used to validate the models.

$$\mathrm{NDWI} = \frac{\rho_{(\lambda_g)} - \rho_{(\lambda_{nir})}}{\rho_{(\lambda_g)} + \rho_{(\lambda_{nir})}} \qquad (2)$$

where $\rho_{(\lambda g)}$ is the green wavelength reflectance; and $\rho_{(\lambda nir)}$ is the near infrared wavelength reflectance.

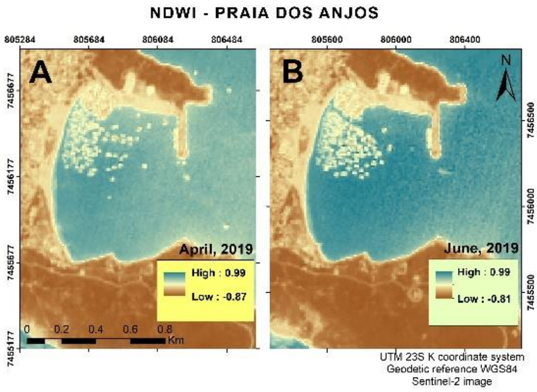

Figure 5. NDWI calculated to separate water and non-water features. (A) NDWI for April 6, 2019. (B) NDWI for June 20, 2019.

Afterwards, a 3x3 low-pass filter was applied to remove noises on the images (Jagalingam et al., 2015; Caballero and Stumpf, 2019; Leder et al., 2019). The next step was the sunglint correction using the algorithm by Hedley et al. (2005). The sunglint correction was applied only in April 6, 2019 image, since June 20, 2019 image did not present this feature. For this, Equation (3) was applied (Hedley et al., 2005):

$$\rho`_{(\lambda i)} = \rho_{(\lambda i)} - b_{(\lambda i)}(\rho_{(\lambda nir)} - M_{(\lambda_{nir})}) \qquad (3)$$

where $\rho`_{(\lambda i)}$ is the sunglint corrected pixel for wavelength *i*; $\rho_{(\lambda i)}$ is the reflectance of the wavelength *i*; $b_{(\lambda i)}$ is the regression slope; and $M_{(\lambda nir)}$ is the minimum value of the infrared wavelength.

With the pre-processed images, the log-transformed band ratio algorithm by Stumpf et al. (2003) could be applied. The model uses a log-transformed ratio of the reflectance of bands with different absorption by the water (blue and green) and, therefore, the result of this ratio will change with depth. In this way, one band will have arithmetically lower values than another. As the reflectance of both bands decreases with increasing depth, the ln (ρ (λ)) of the band with greater absorption (green) will decrease proportionally faster than the ln (ρ (λ)) of the band with less absorption (blue) (Stumpf et al., 2003). Thus, the greater the depth, the greater the value of this ratio (Caballero and Stumpf, 2019).

$$\mathrm{SDB} = m_1 * (\mathrm{pSDB}) - m_0 \qquad (4)$$

$$\mathrm{pSDB} = \frac{ln(n\rho_{(\lambda b)})}{ln(n\rho_{(\lambda g)})} \qquad (5)$$

where SDB is the Satellite-Derived Bathymetry (in meters); pSDB is the “pseudo” depth by satellite (dimensionless); *n* is a fixed constant for the entire area to ensure that the logarithms are positive; $\rho_{(\lambda b)}$ is blue wavelength reflectance; m_1 and m_0 are the scale and offset respectively.

This model was originally developed as an alternative solution to Lyzenga (1978) method for mapping large areas of coral reefs (atolls) in Hawaii, requiring less empirical parameters (just known depth points) and also because it can be applied in different types of seabed (albedo) (Stumpf et al., 2003). Thus, this algorithm is applied in different types of coastal environments (Table 1). After calculating pSDB, the linear Pearson`s correlation (*r*) and the linear regression was calculated with previously separated control points (pSDB x control points).

The model calibrations were performed only in the regions without boats on the images, that is, in pixels referring to water. Correlations were analyzed for different depth intervals: 1-4m; 4-8m; 8-13m; 4-13m and 1–13m. From the linear correlation covering the largest depth range (1-13m), the trend line equation for determining SDB was generated for each date separately (April 6 and June 20, 2019), as well as the r^2 determination coefficients.

In addition to pSDB calculation using the blue and green bands, replacement of the green by red band was evaluated to estimate depths in 1-4 m depth range. As indicated and tested by Caballero and Stumpf (2019), the use of the red wavelength can provide better information at depths shallower than 6-8 m, since it attenuates faster than the green.

The equations for generating the SDB were applied for each date. As a solution to estimate depths in regions where there are vessels, the SDB (a raster file) was converted into points and interpolated for the entire area using the Topo to Raster tool on ArcGIS 10.0.

Subsequently, the estimated depths were correlated with the previously separated check points (SDB x check points) for validation and analysis of statistical parameters such as Pearson`s correlation *r*, coefficient of determination r^2, Mean, Standard Deviation, Mean Absolute Error (MAE) and Root Mean Square Error (RMSE) (e.g. Evagorou et al., 2019; Yunus et al., 2019).

Results

The NDWI (Figure 5) allowed the separation of water and non-water pixels, serving to mask vessels in the area and, consequently, not to assign values to these pixels in the models. For April 6th 2019, after calculating the pSDB, the correlation with the control points was generated (Figure 6).

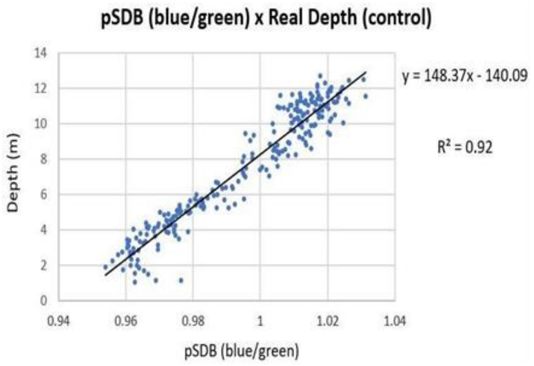

Figure 6. Scatterplot between the natural logarithmic ratio of blue and green bands (pSDB) and depth control points in meters (n = 241). April 6, 2019.

The scatterplot between pSDB and control points, calibrated for the area without boats on the image (only water pixels), showed a strong linear correlation, highlighting an important association between the images and depths in the study area. It is worth noting that, a necessary procedure in this type of study is to evaluate and determine the extinction depth by the behavior of the values in the graph, that is, to determine a depth at which the variables no longer correlate linearly (Guerreiro and Moura, 2015; Zwolak et al., 2020). However, this behavior was not observed in Figure 6, which allowed the processing and statistical analysis to be performed considering the largest depth interval (1-13 m). Table 3 shows r and r^2 values for all depth intervals evaluated with blue/green bands and also for specific 1-4 m interval with blue/red bands.

Table 3 - Correlation and determination coefficients and p-value for different depth intervals. April 6, 2019.

pSDB (blue/green) x Depth (control)	*r*	r^2	*n*	*p-value for r*
1 – 4 m	0.331	0.109	42	$p < 0.05$
4 – 8 m	0.954	0.910	74	$p < 0.05$
8 – 13 m	0.657	0.432	125	$p < 0.05$
4 – 13 m	0.947	0.897	199	$p < 0.05$
1 – 13 m	0.963	0.927	241	$p < 0.05$
pSDB (blue/red) x Depth (control)	-	-	-	-
1 – 4 m	0.897	0.804	42	$p < 0.05$

The linear trend line equation (Figure 6) was applied to generate the SDB on Praia dos Anjos for the region without boats (a 10 m of spatial resolution raster). However, considering a weak correlation in the 1-4 m depth interval with blue and green bands (Table 3), the generated SDB was converted into points and the values less than 4 m were replaced by those obtained with the red wavelength. After joining, the points were interpolated with Topo to Raster tool in ArcGIS 10.0 for the entire area in order to cover the region with boats (Figure 7).

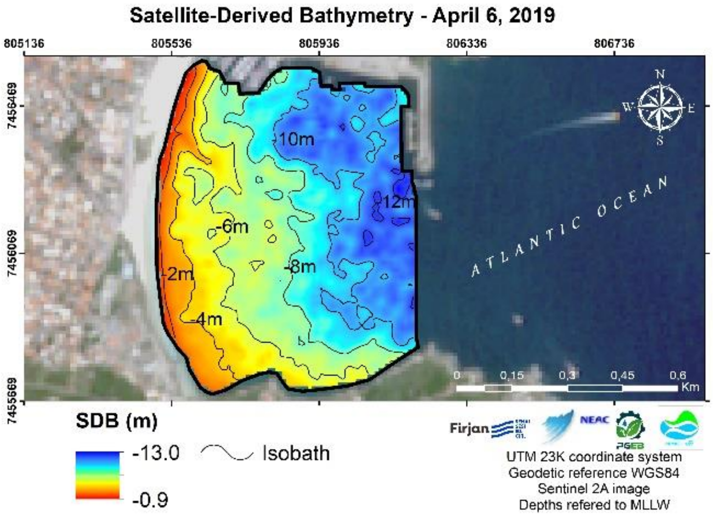

Figure 7. Satellite-Derived Bathymetry (SDB) on Praia dos Anjos. Depths in meters. April 6, 2019.

The generated model (Figure 7) was able to assign depth values for each pixel of the image, showing shallower regions near the beach, intermediate and deeper regions near Forno Port, as it moves away from the shoreline. The navigation channel near Forno Port is evident by deeper waters. However, the model was evaluated by previously separated check points, allowing statistical analysis of errors. The correlation of the estimated bathymetry (SDB) and check points was calculated (Figure 8).

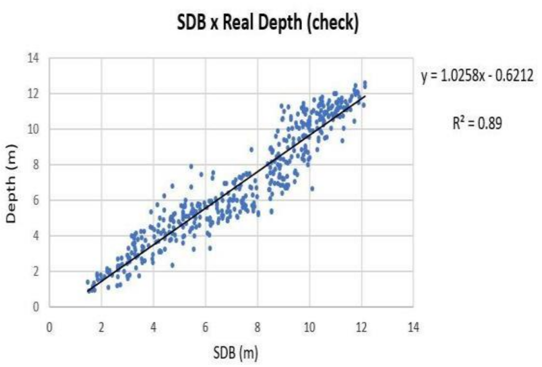

Figure 8. Scatterplot between SDB and check points in meters (n = 451). April 6, 2019.

The graph (Figure 8) shows a strong correlation between the real and satellite-derived bathymetry (r = 0.945 and r^2 = 0.893). Equally, r and r^2 were determined for each depth interval assessed, as well as the statistical errors (Tables 4 and 5).

It is noticed that the mean depths of the SDB and *in situ* depth (check points) were close, as well as the standard deviation. Additionally, a RMSE of 1.095 m was found for this model.

For June 20, 2019, the correlation between pSDB and control points generated the following graph (Figure 9):

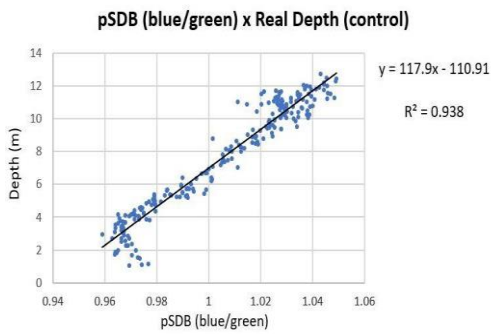

Figure 9. Scatterplot between the natural logarithmic ratio of blue and green bands (pSDB) and depth control points in meters (n = 239). June 20, 2019.

Figure 9 shows a strong correlation (r = 0.969 and r^2 = 0.938) between the variables for 1-13 m depth interval. Likewise, no extinction depth was observed. r and r^2 values for each depth interval are shown in Table 6.

In the same way as observed in April model, the linear trend line equation shown in Figure 9 was applied to generate the SDB on Praia dos Anjos for the region without boats. The depths in 1-4 m interval also show a weak (and negative) correlation with the blue and green bands and a strong correlation with blue and red bands ratio (Table 6). Therefore, the SDB generated for June was converted into points and the values shallower than 4 m were replaced by those obtained by the red wavelength and interpolated for the entire area (Figure 10).

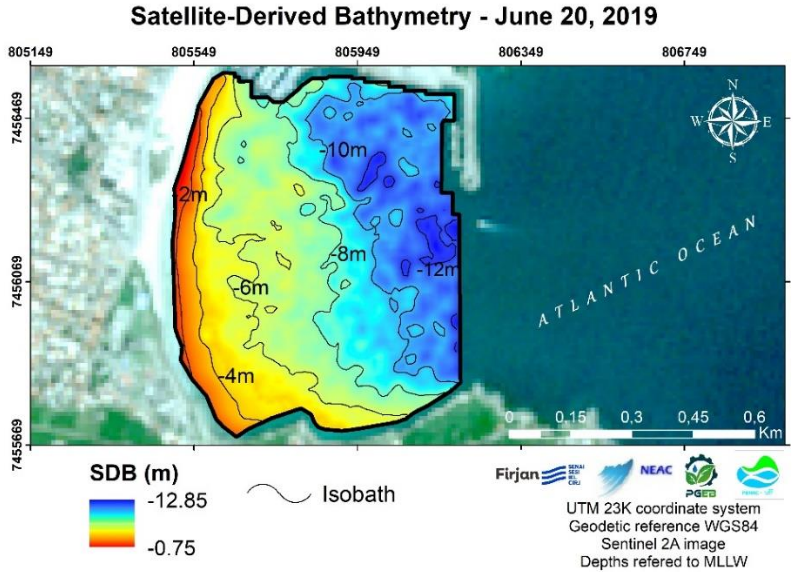

Figure 10. Satellite-Derived Bathymetry on Praia dos Anjos. Depths in meters. June 20, 2019.

The SDB for June 20, 2019 was also able to distinguish shallow regions close to the coast and deeper as it moves away from the beach, as well as the port navigation channel with deeper waters. Comparing Figures 7 and 10, similar depth values on the models can be observed. The correlation of the estimated values (SDB) and check points for the entire area in June 20, 2019 generated the following graph (Figure 11):

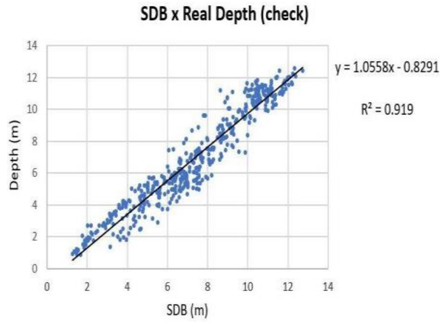

Figure 11. Scatterplot between estimated depth (SDB) in meters and depth check points in meters (n = 450). June 20, 2019.

The SDB and checkpoints mean values were close for June model, as well as the standard deviation. A RMSE of 0.98 m was obtained. Comparing Tables 5 and 8, the statistical parameters were similar for both models (April and June), with a RMSE ≅1.0.

Table 4 - Correlation and determination coefficients and p-value for different depth intervals between SDB and check points. April 6, 2019.

SDB x Depth (check)	*r*	r^2	*n*	*p-value for r*
1 – 4 m	0.761	0.597	84	$p < 0.05$
4 – 8 m	0.726	0.526	199	$p < 0.05$

8 – 13 m	0.725	0.526	168	$p < 0.05$
4 – 13 m	0.906	0.822	367	$p < 0.05$
1 – 13 m	0.945	0.893	451	$p < 0.05$

Table 5 - Statistical parameters and errors of Satellite-Derived Bathymetry on April 6 2019 (given in meters).

Statistcs and erros	**Mean**	**Standard Deviation**	**Mean Absolute Error**	**Root Mean Square Error**	**n**
SDB (1 – 13 m)	7.33	2.83	0.43	1.095	451
In situ depth - check (1 – 13 m)	6.89	3.07			

Table 6 - Correlation and determination coefficients and p-value for different depth intervals. June 20, 2019.

pSDB (blue/green) x Depth (control)	*r*	r^2	*n*	*p-value for r*
1 – 4 m	-0.192	0.037	42	It is not significance at $p < 0.05$
4 – 8 m	0.940	0.883	74	$p < 0.05$
8 – 13 m	0.771	0.595	123	$p < 0.05$
4 – 13 m	0.963	0.928	197	$p < 0.05$
1 – 13 m	0.969	0.938	239	$p < 0.05$
pSDB (blue/red) x Depth (control)	-	-	-	-
1 – 4 m	0.944	0.891	42	$p < 0.05$

Table 7 - Correlation and determination coefficients and p-value for different depth intervals between SDB and check points. June 20, 2019.

SDB x Depth (check)	*r*	r^2	*n*	*p-value for r*
1 – 4 m	0.758	0.575	82	$p < 0.05$
4 – 8 m	0.758	0.574	199	$p < 0.05$

8 – 13 m	0.805	0.648	169	$p < 0.05$
4 – 13 m	0.937	0.879	368	$p < 0.05$
1 – 13 m	0.959	0.919	450	$p < 0.05$

Table 8 - Statistical parameters and errors of Satellite-Derived Bathymetry on Juno 20, 2019 (given in meters).

<table>
<tr><th>Statistcs and erros</th><th>Mean</th><th>Standard Deviation</th><th>Mean Absolute Error</th><th>Root Mean Square Error</th><th>n</th></tr>
<tr><td>SDB
(1 – 13 m)</td><td>7.35</td><td>2.785</td><td rowspan="2">0.42</td><td rowspan="2">0.98</td><td rowspan="2">450</td></tr>
<tr><td>In situ depth - check
(1 – 13 m)</td><td>6.92</td><td>3.067</td></tr>
</table>

Discussion

The results of this study demonstrated the potential of Sentinel-2 images to estimate bathymetry in the coastal waters of Arraial do Cabo, on Praia dos Anjos, with strong correlations between the images and known depth values, considering an interval of 1-13 m in two distinct periods. In general, both images used (Sentinel-2A and B) showed similar statistical results.

The results presented here are similar to those found by Caballero and Stumpf (2019) in South Florida, which the authors presented r^2 values from 0.74 to 0.93 between the blue/green band ratios and control points in an interval of 1-18 m depth for different dates using Sentinel-2 images. However, these authors used LIDAR data and nautical charts to calibrate and validate the models, different sources than the data used in this study (echosounding).

In addition, Caballero and Stumpf (2019) presented a model error value of approximately 0.5, being close to those found at Praia dos Anjos (RMSE $\cong$ 1.0). On the other hand, these authors demonstrated the possibility of generating models with only 5-10 calibration points, which is advantageous for the reduction of costs and time in bathymetric surveys.

Casal et al. (2019) also presented similar results to this study and to Caballero and Stumpf (2019). The authors evaluated the band ratio model to estimate depths using Sentinel-2 images in Dublin Bay and Mulroy Bay, these being estuarine and marine fiordic inlet environments in Ireland. r values from 0.8 to 0.88 were found between the band ratios and depth points measured in field in the range of 0-10 m on five different image dates.

Regarding the bathymetric models (SDB) generated by Casal et al. (2019), these presented values of r^2 ranging from 0.720 to 0.833 between the estimated depths and check points, and RMSE between 0.963 and 1.453. Although these r^2 values are slightly lower than those found in this study at Praia dos Anjos (r^2 = 0.893 and 0.919), the authors concluded that Sentinel-2 images were efficient for bathymetric mapping on the coast of Ireland.

Another study that used Sentinel-2 images for bathymetric mapping was that by Evagorou et al. (2019). The authors evaluated the images over a 12-month time series in Cyprus (Mediterranean Sea) and found r^2 from 0.81 to 0.95 between the estimated depths and check points in an interval of 0-22 m, and RMSE from 1.39 to 2.56 m. The r^2 values presented by Evagorou et al. (2019) with the methodology of the log-transformed ratio band model were also close to those found in this study, although these authors obtained higher RMSE values (for Praia dos Anjos, RMSE were 1.095 and 0.98 for April and June respectively).

In Kenya, Kimeli et al. (2018) evaluated Landsat 8 images to estimate depths in Mombasa Port Channel using data from nautical charts. The authors applied the blue/green band ratio and obtained depths up to 10 m with $r^2 \cong 0.9$ and RMSE of 1.61 m. These results are also similar to those of this study, although the authors used others field and satellite data.

However, an important point to be highlighted is the fact that the blue/red band ratio has a greater correlation with shallower depths, or even the yellow band from Worldview Satellite demonstrated by Chénier et al. (2018). This fact seems to happen in several cases, as indicated by Caballero and Stumpf (2019), Caballero and Stumpf (2020) and Muzirafuti et al. (2020), as well as in this study.

Correlations between the blue/green band ratios (pSDB) with calibration points at depths up to 4 m showed weak *r* values for both April (r = 0.331, significant at $p < 0.05$) and June (r = -0.192, not significant at $p < 0.05$) models in this study. Nevertheless, when evaluating the blue/red band ratios at this depth interval, *r* values increased to r = 0.897 and r = 0.944 on April and June respectively, both significant at $p < 0.05$.

Muzirafuti et al. (2020) obtained a slight difference of r^2 values between band ratios in the models using QuickBird images in a 0-6 m deep interval in turbid waters in Adriatic Sea, Italy. The authors state that the estimated depths with the blue/green band ratio showed better results in relatively deeper waters and worse results in shallower waters close to the shoreline. However, the evaluated blue/red band ratio model showed r^2 = 0.9108 with RMSE = 0.32 m and r^2 = 0.8682 and RMSE = 0.518 for the blue/green band ratio.

Caballero and Sumpf (2019) also highlights this situation, finding similar results. The authors indicate that the blue/red band ratio model was more sensitive at depths of up to 5-6 m. They found r^2 values from 0.8 to 0.99 between the blue/red band ratio and calibration points in 0-6 m depth interval. Also, as done in our study, it is suggested a combination and integration of the blue/red band ratio to estimate shallower depths and blue/green band ratio for deeper regions.

Chénier et al. (2018) also obtained and evaluated this situation with Worldview-2 and 3 images, even in an arctic environment in Canada. However, the authors used blue/green and blue/yellow band ratios to estimate depths. In all examined cases, lower RMSE was found in the models when using a blue/yellow banding ratio, ranging from 0.3 to 0.95 m (0-2 m depth interval) and 0.43 to 0.78 m (2-4 m depth interval). Models using blue/green band ratio, RMSE were from 0.44 to 1.31 m and 0.5 to 1.09 m at the same depth intervals respectively.

Therefore, Chénier et al. (2018) states that the use of the yellow band presents better results for depths of up to 4m and the green band for greater depth, as well as also suggest the combination and integration of these bands to estimate bathymetry.

This fact, observed in our study at Praia dos Anjos, seems to be due to an interference and high reflectance of the green light by the bed in shallow waters, since it has a capacity of penetration in water greater than the red light (Caballero and Stumpf, 2019). Thus, once the red light is more quickly absorbed it may have less bed interference.

Thus, the results obtained for Praia dos Anjos in Arraial do Cabo, RJ, are close to those demonstrated in other countries, with different satellites and coastal environments investigated in the literature. However, environmental conditions like the water transparency or turbity; water quality; phytoplankton (chlorophyll a), dissolved organic substances and the presence of sediment are key factors that determine the penetration of light into the water, as well as the presence of clouds and sunglint in the images used (Jagalingam et al., 2015; Tang and Mahmud, 2018). So, due to its clear waters and low sediment discharge by rivers in the region, the environmental conditions at Praia dos Anjos possibly contributed positively to the results achieved between the images and *in situ* measured depths.

Conclusions

This study showed the application of remote sensing to estimate depths in a clear water coastal environment, since bathymetric information is essential for several applications of environmental monitoring and coastal engineering works. Orbital images offer an alternative and a complement to hydrographic studies, in which depths are evaluated and tested in different types of coastal environments worldwide.

Although the satellites of the Sentinel-2 mission proved effective for this purpose in the area with the employed methodology, the use of such models for navigation is not recommended, because uncertainties expected are not adequate. However, these can be a quick alternative to assess submerged features and reduce field measurement time and costs.

Both models (April and June) for Sentinel-2A and B showed a strong correlation between the estimated depth values (SDB) and check points $r^2 \cong$ 0.9. However, the use of the red wavelength was essential to obtain better results at depths shallower than 4 m. In addition, the absence of clouds on the images over the study area and the water quality contributed positively to the results achieved.

In this study, an extinction depth up to 13 m was not observed. Thus, in future studies, depths greater than 13 m can be evaluated for deeper areas behind the port breakwater, since this work was limited to the Forno Port area.

Further tests are recommended to improve the models. Likewise, it is recommended that the calibrated equations should be applied and tested for later dates and perform only an assessment with new check points and, once the model is no longer effective, it will be necessary a new calibration. In addition, this approach can be applied and evaluated for other nearby regions in coral reefs environments for mapping ecosystems.

Lastly, remote sensing has the ability to estimate depths at which it can be used for bathymetric mappings in clear waters. Thus, it can be integrated into port environmental monitoring programs as an effective and low-cost alternative, being complementary to hydrographic surveys on Praia dos Anjos.

Acknowledgements

The authors thank the Industry Federation of the State of Rio de Janeiro (FIRJAN) for the support and financing the field work activities. Thanks to the Federal Fluminense University (UFF) where part of this work was developed and to the Nucleus of Studies in Coastal Environments (NEAC). Thanks to the European Space Agency for free distributing Sentinel-2 images. This work is derived from the Forno Port environmental monitoring program funded by FIRJAN. JCW is grateful to CNPq for a Research fellowship (grand # 306714/2013-).

References

Abualhin, K., Niemeyer, I., 2018. Deriving bathymetric maps of the shallow coastal water of the Gaza Strip Zone using passive remotely sensed imagery. Journal of the Indian Society of Remote Sensing 46, 1341-1351.

Areias, C., Spotorno-Oliveira, P., Bassi, D., Iryu, Y., Nash, M., Castro, J.V.A., Tâmega, F.T.S., 2020. Holocene sea-surface temperatures and related coastal upwelling regime recorded by vermetid assemblages, southeastern Brazil (Arraial do Cabo, RJ). Marine Geology 425.

Barbiére, E.B., 1975. Ritmo climático e extração de sal em Cabo Frio. Revista Brasileira de Geografia 37, 23-109.

Barbosa, D.S., Anjos, A.P.A., Albuquerque, A.L.S., Sifeddine, A., 2003. Sedimentação orgânica na Lagoa Brejo do Espinho, Cabo Frio (RJ): Composição e implicações paleoclimáticas. Paper presented at the IX Congresso da Associação Brasileira de Estudos do Quaternário, Recife, Brasil.

Basith, A., Prastyani, R., 2020. Evaluating Acomp, Flaash and Quac on Worldview-3 for Satellite Derived Bathymetry (SDB) in shallow water. Geodesy and Cartography 46, 151-158.

Bitan, M., Zviely, D., 2020. Sand beach nourishment: Experience from the Mediterranean Coast of Israel. Journal of Marine Science and Engineering 8.

Caballero, I., Stumpf, R.P., 2019. Retrieval of nearshore bathymetry from Sentinel-2A and 2B satélites in South Florida coastal waters. Estuarine, Coastal and Shelf Science 226, 1-12.

Caballero, I., Stumpf, R.P., 2020. Towards routine mapping of shallow bathymetry in environments with variable turbidity: Contribution of Sentinel-2A/B satellites mission. Remote Sensing 12, 1-23.

Carvalho, L.L., Dias, F.F., Souza, V.S.M., Silva, A.L., Santos, P.R.A., Vargas, R., Villaça, R. C., 2018. Solução de baixo custo para correção de variações de maré no mapeamento de ambientes costeiros. Revista Brasileira de Geografia Física 11, 904-912.

Casal, G., Monteys, X., Hedley, J., Harris, P., Cahalane, C., McCarthy, T., 2019. Assessment of empirical algorithms for bathymetry extraction using Sentinel-2 data. International Journal of Remote Sensing 40, 2855-2879.

Chénier, R., Faucherr, M-A., Ahola, R., 2018. Satellite-derived bathymetry for improving canadian hydrographic service charts. International Journal of Geo-Information 7, 1-15.

Coe, H.H.G., Carvalho, C.N., 2013. Cabo Frio – Um enclave semiárido no litoral úmido do estado do

Rio de Janeiro: Respostas do clima atual e da vegetação pretérita. GEOUSP – espaço e tempo 17, 136-151.

Colaço, G., Violante-Carvalho, N., Arruda, W.Z., D`Avila, V., Vilhena, H., Filippo, A., Candella, R., 2021. Mid-long term characterization and short term modelling of a semi-protect pocket sandy beach in the southern coast of Brazil. Regional Studies in Marine Science 41.

Conti, L.A., Mota, G.T., Barcellos, R.L., 2020. High-resolution optical remote sensing for coastal benthic habitat mapping: A case study of the Suape Estuarine-Bay, Pernambuco, Brazil. Ocean and Coastal Management 193.

Dias, L.F.L., Castro, J.V.W., Seoane, J.C.S., 2014. Transição Pleistoceno-Holoceno na Enseada dos Anjos, Arraial do Cabo/Rio de Janeiro: Reconstituição paleoambiental 3D. Revista Brasileira de Cartografia 66, 931-951.

Dierssen, H.M., Zimmerman, R.C., Leathers, R.A., Downes, T.V., Davis, C.O., 2003. Ocean color remote sensing of seagrass and bathymetry in the Bahamas Banks by high- resolution airborne imagery. Limnology and Oceanography 48, 444-455.

ESA - European Space Agency, 2015. Sentinel-2 User Handbook. Paris: ESA.

Evagorou, E., Mettas, C., Agapiou, A., Themistocleous, K., Hadjimitsis, D., 2019. Bathymetric maps from multi-temporal analysis of Sentinel-2 data: the case study of Limassol, Cyprus. Advances in Geoscience 45, 397-407.

Figueiredo Jr, A. G., Pacheco, C.E.P., Vasconcelos, S.D., Silva, F.T., 2015. Geomorfologia e sedimentologia da plataforma continental, in: Kowsmann, R.O. (Ed.), Geologia e geomorfologia. Elsevier, Rio de Janeiro, pp. 13-32.

Gao, J., 2009. Bathymetry mapping by means of remote sensing: methods, accuracy and limitations. Progress in Physical Geography 33, 103-116.

Green, E., Edwards, A., Mumby, P., 2000. Mapping bathymetry, in: Edwards, A.J. (Ed.), Remote sensing handbook for tropical coastal management. UNESCO Publishing, Paris, pp. 219-233.

Guerreiro, R., Moura, A., 2015. Aplicação de uma metodologia de derivação de batimetria a partir de imagens de satélites. Paper presented at the VIII Conferência Nacional de Cartografia e Geodésia, Portugal.

Habermann, L., Vincentelli, M.G.C., Contreras, S.A.C., Perinotto, J.A.J., 2018. Caracterização geológica da distribuição de reservatórios carbonáticos albianos, sudoeste da Bacia de Campos (Brasil). Geociências 37, 279-298.

Hedley, J.D., Harborne, A.R., Mumby, P.J., 2005. Technical note: Simple and robust removal of sun glint for mapping shallow-water benthos. International Journal of Remote Sensing 26, 2107–2112.

Henrico, I., Bezuidenhout, J., 2020. Determining the change in the bathymetry of Saldanha Bay due to harbour construction in the seventies. South African Journal of Geomatics 9, 236-249.

International Hydrographic Organization – IHO. 2005. Manual on hydrography. Monaco: International Hydrographic Bureau.

Jagalingam, P., Akshaya, B.J., Hedge, A.V., 2015. Bathymetric mapping using Landsat 8 satellite imagery. Procedia Engineering 116, 560-566.

Jupp, D., 1988. Background and extension to depth of penetration (DOP) mapping in shallow coastal waters. Paper presented at the Proceedings of the symposium on remote sensing of the coastal zone, Gold Coast, Queensland.

Kimeli, A., Thoya, P., Ngisiang`e, N., Ong`anda, H., Magori, M., 2018. Satellite-derived bathymetry: a case study of Mombasa Port Channel and its approaches, Kenya. WIO Journal of Marine Science 17, 93-102.

Leder, T.D., Leder, N., Peroš, J., 2019. Satellite derived bathymetry survey method – example of Hramira Bay. Transactions of Maritime Science 8, 99-108.

Lyzenga, D.R., 1978. Passive remote sensing techniques for mapping water depth and bottom features. Applied Optics 17, 379-383.

Lyzenga, D.R., 1985. Shallow-water Bathymetry using combined LiDAR and Passive Multispectral Scanner Data. International Journal of Remote Sensing 6, 115–125.

Mateo-Pérez, V., Corral-Bobadilla, M., Ortega-Fernández, F., Vergara-González, E.P., 2020. Port bathymetry Mapping using support vector machine technique and Sentinel-2 satellite imagery. Remote Sensing 12.

McFeeters, S.K., 1996. The use of normalized difference water index (NDWI) in the delineation of open water features. International Journal of Remote Sensing 17, 1425-1432.

Melo, L.V., Sales, T.B., Souza, G.L., Brant, F.F., Manicacci, M., 2009. Ampliação do Porto do Forno na Reserva Extrativista Marinha em Arraial do Cabo-RJ. Boletim do Observatório Ambiental Alberto Ribeiro Lamego 3, 163-186.

Motta, P.R., Netto, L.R., Bastos, E.B., Pereira, T.G., Bulhões, E.M.R., 2018. Distribuição e transporte de sedimentos costeiros exemplos em Arraial do Cabo, RJ. Revista Brasileira de Geomorfologia 19, 341-358.

Muehe, D., 1998. O litoral brasileiro e sua compartimentação, in: Cunha, S.B., Guerra, A.J.T. (Orgs.), Geomorfologia do Brasil. Bertrand Brasil, Rio de Janeiro, pp. 273-349.

Mumby, P., Edwards, A., 2000. Remote sensing objectives of coastal managers, in: Edwards, A.J. (Ed.), Remote sensing handbook for tropical coastal management. UNESCO Publishing, Paris, pp. 31-39.

Muzirafuti, A., Barreca, G., Crupi, A., Faina, G., Paltrinieri, D., Lanza, S., Randazzo, G., 2020. The contribution of multispectral satellite image to shallow water bathymetry mapping on the coast of Misano Adriatico, Italy. Journal of Marine Science and Engineering 8, 1-21.

Novo, E.M.L.M., 2010. *Sensoriamento remoto: princípios e aplicações*. São Paulo: Blucher.

Parente, C., Pepe, M., 2018. Bathymetry from Worldview-3 satellite data using radiometric band ratio. Acta Polytechnica 58, 109-117.

Quadros, P., Castro, J.W.A., Guedes, E., Pereira, V.C.R., 2016. Distribuição sazonal dos sedimentos na praia do Farol, Ilha do Cabo Frio, Arraial do Cabo, Rio de Janeiro. Revista Brasileira de Geomorfologia 17, 389-398.

Riccomini, C., Sant`Anna, L.G., Tassinari, C.C.G., 2012. Pré-sal: geologia e exploração. Revista USP (95), 33-42.

Savi, D.C., 2007. Erosão e acresção costeira na enseada dos Anjos, Arraial do Cabo, RJ. Revista Brasileira de Geofísica 25, 91-99.

Silva, A.C., 2009. Dinâmica batimétrica e sedimentológica da região de Cabo Frio – estado do Rio de Janeiro. Tese (Doutorado). Rio de Janeiro, UFRJ.

Simões, I.C.V.P., 2007. Aplicação da batimetria multifeixe para definição da morfologia detalhada do fundo marinho ao largo da Laguna de Araruama e Arraial do Cabo-RJ. Dissertação (Mestrado). Niterói, UFF.

Simpson, C.E., Arp, C.D., Sheng, Y., Carroll, M.L., Jones, B.M., Smith, L., 2021. Landsat-derived bathymetry of lakes on the Arctic coastal plains of northern Alaska. Earth System Science Data 13, 1135-1150.

Smith, W.H.F., Sandwell, D.T., 2014. Conventional bathymetry, bathymetry from space, and geodetic altimetry. Oceanography 17, 8-23.

Stumpf, R.P., Holderied, K., Sinclair, M., 2003. Determination of water depth with high-resolution satellite imagery over variable bottom types. Limnology and Oceanography 48, 547-556.

Tang, K. K. W., Mahmud, M.R., 2018. Imagery-derived bathymetry in Strait of Johor`s turbid Waters using multispectral images. Paper presented at The International Archives of the Photogrammetry, Remote Sensing and Spatial Information Sciences and the International Conference on Geomatics and Geospatial Technology, Kuala Lumpur, Malaysia.

Vargas, R., Dias, F.F., Wasserman, J.C.F.A., Santos, P.R.A., Silva, A.L., Santos, C.A., Ferreira, V.L.D., Barcelos, J.S., 2020. Mapeamento topobatimétrico do canal de maré da Lagoa de Araruama, Rio de Janeiro, Brasil, in: Paula, D.P., Dias, J.A., Fonseca, L.C., Rodrigues, M.A.C., Albuquerque, M.G., Palma, M., Pereira, S.D. (Eds.), Diálogos em torno da linha de costa: O oceano que nos une. FGEL-UERJ, Rio de Janeiro, pp. 51-62.

Venancio, K.K., Garcia, P.D., Gireli, T.Z., Corrêa, T.B., 2020. Hydrodynamic modeling with scenario approach in the evaluation of dredging impacts on coastal erosion in Santos (Brazil). Ocean and Coastal Management 195.

Wei, C., Theuerkauf, S.J., 2021. A novel multitemporal approach for Satellite-Derived Bathymetry for coastal water of Palau. Journal of Coastal Research 37, 336-348.

Westley, K., 2021. Satellite-Derived Bathymetry for maritime archaeology: Testing its effectiveness at two ancient harbours in the Eastern Mediterranean. Journal of Archaeological Science: Reports 38.

Yunus, A.P., Dou, J., Song, X., Avtar, R., 2019. Improved bathymetric mapping of coastal and lake environments using Sentinel-2 and Landsat-8 images. Sensors 19, 1-20.

Zwolak, K., Marchel, Ł., Skóra, M., Przybysz, R., Jóźwiak, R., Tomaszewska, K., 2020. Accessibility and usability of Landsat 8 data for the purpose of satellite-derived bathymetry of the South Baltic near-shore waters on the example of Gulf of Gdańsk. Scientific Journal of Polish Naval Academy 220-221, 29-46.